ROYAL SOCIETY OF CHEMISTRY

Proofing your Book Chapter

The following contains the PDF proof of your book chapter for you to review. Please follow the steps below to proof your chapter.

1. Read through your chapter carefully

- Remember to check that:
  - **special characters** appear correctly, especially in equations
  - **Figures and Tables** are correct
  - **headings and sub-headings** are placed correctly
- Our staff will not read through your chapter in detail once you have returned it, so please make sure you have checked everything. Final responsibility for content lies with the author.
- As no revised proofs will be provided, please ensure all required corrections are indicated at this stage.

2. Mark up any corrections that are required

- Please only correct scientific or grammatical errors in your chapter – **do not** rewrite sections or make minor cosmetic changes at this stage.
- Please use the **annotation tools** to mark up corrections on the PDF proof – further instructions can be found on the following page.
- Please do not edit the PDF directly or send a list of corrections.
- If any replacement figures are required, please resupply the file at the highest possible resolution.
- Please **only supply new versions of figures if you have been requested to do so, or you need to supply a corrected version.**
- Permission statements for reproduced material may have been edited to meet the different requirements of the copyright holders. Please do not correct the formatting of these statements.

3. Make sure you have answered all author queries

- These are listed before the beginning of the chapter – click on the query number to jump to the relevant place in the text.
- **Please put your responses in the text, not on the query page.**

4. Return your corrected proof to your editor(s)

- Please email the annotated PDF of your chapter to h.azevedo@qmul.ac.uk; jmano@ua.pt; joaoborges@ua.pt within **ONE WEEK** of receipt.
- Please do not return the PDF to Books Production, or to the email address from which you received the download link.

If you have any queries, please do not hesitate to contact me at kumudhavalli.n@mpslimited.com

How to Annotate your PDF Proof

Note: The location and appearance of tools may vary depending on the software you are using to read your proof. We recommend using Adobe Acrobat Reader DC (as shown in the screenshots below), which can be downloaded for free online.

The **Comment** function can be found in the **right-hand sidebar**, which should appear when you open your PDF.
Otherwise, in the View menu, click '**Tools**' and then select '**Comment**'. This will make the **Comment tools** visible (shown below).

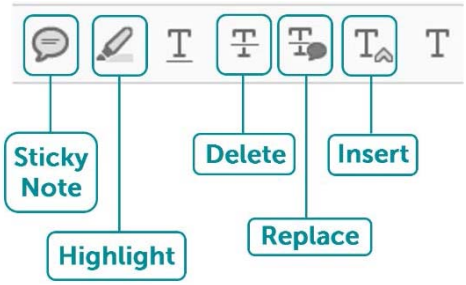

Select the piece of text that you want to mark up, and then click on the relevant Tool button to add the mark up to the text.

For the Insert, Replace, and Sticky Note tools, this will open up a Note in **which you can add instructions, or the text to be replaced/inserted –** otherwise, you can double-click on the mark-up to open this.

For all tools, any instructions you've added will appear in the Comment sidebar – you can also double-click on this to change, add to or remove the instructions.

Replace

Use the Replace tool to indicate text that should be changed.

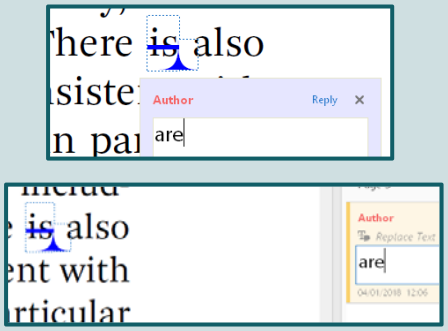

Insert

Use the Insert tool to provide new text.

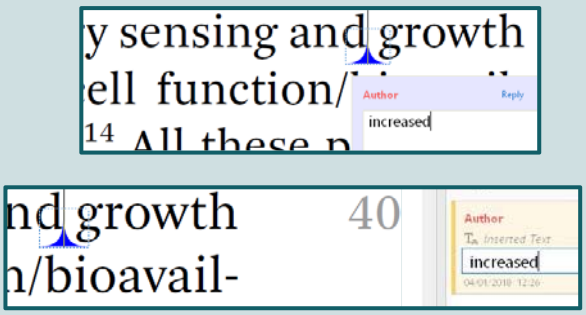

Delete

Use the Delete tool to indicate text that needs to be removed completely.

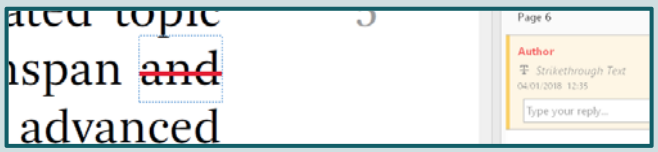

Highlight

Use the Highlight tool to indicate formatting changes to text.

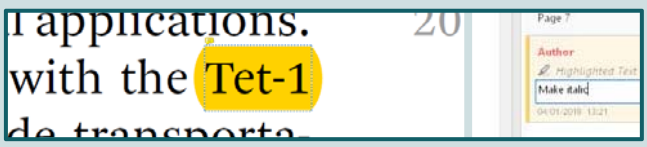

Sticky Note

Use the Sticky Note tool to respond to a query, or indicate a change that cannot be marked up using one of the tools above.

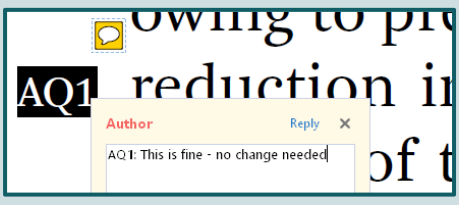

Hints and tips

Special characters can be pasted into corrections from the Character Map in your operating system.

Text can be made **bold** and **italic** using shortcut keys Ctrl+B and Ctrl+I.

If you have difficulty selecting all the text you wish to correct, try holding down the Shift key and using the arrow keys.

AUTHOR QUERY FORM

Book Title: Soft Matter for Biomedical Applications
Chapter 18

Please indicate the changes required in response to the queries within the text. If no changes are needed please clearly state this next to the query marker.

TS1	The running head has been shortened to fit the space available. Please check that the text is suitable.

Abstract

The abstract for your chapter is reproduced below for your reference. Please note that this will **not** appear in the final printed version of your chapter.

Layer-by-layer (LbL) assembly is an easier, inexpensive, and highly versatile bottom-up methodology to modify surfaces and fabricate functional multilayer thin films and nanocomposites with fine-tuned compositions, structures, properties, and functions at the nanoscale. Since the early stages of its development, LbL technology has gathered increasing attention across different fields of application, including in the biomedical field owing to its mild processing conditions. In this chapter, we review the multitude of templates, spanning from the zero-dimensional to the three-dimensional, for shaping a diverse set of multifunctional soft-based LbL structures aiming for biomedical applications. Several examples are given on multilayered structures, including nano-to-macro particles and hollow capsules or tubes, multilayered thin films and free-standing membranes, multicompartmentalized systems, porous scaffolds, and even dynamic living cell platforms, which can act as unprecedented building blocks to create highly complex LbL devices. We envisage that such a multitude of functional LbL devices will stimulate scientists to pursue the further development of LbL technology and foster its effective translation to practical biomedical applications.

CHAPTER 18

Shaping Soft Structures Using Bottom-up Layer-by-layer Assembly Technology for Biomedical Applications

J. BORGES,* C. F. V. SOUSA, I. M. BJØRGE, S. NADINE, C. R. CORREIA, S. G. PATRÍCIO AND J. F. MANO

CICECO – Aveiro Institute of Materials, Department of Chemistry, University of Aveiro, Campus Universitário de Santiago, 3810-193 Aveiro, Portugal
*Email: joaoborges@ua.pt

18.1 Introduction – Overview of the Layer-by-layer Assembly Technology

Over the last three decades, the layer-by-layer (LbL) assembly technology has proven to be a simple, cost-effective, reproducible, and highly versatile bottom-up methodology to functionalize surfaces and fabricate robust and conformal multilayered architectures with precisely tailored compositions, structures, properties, and functions at the nanoscale. The simplicity of the LbL technique relies on the sequential deposition of complementary multivalent materials on a substrate into a diverse set of LbL structures. Dating back to the seminal work by Iler on the fabrication of electrostatically-driven multilayers of oppositely-charged colloidal particles on flat glass substrates in 1966,[1] the LbL assembly technique only started to be recognized after the work by Decher, Hong, and co-workers on the build-up of multilayers of

Soft Matter Series No. 13
Soft Matter for Biomedical Applications
Edited by Helena S. Azevedo, João F. Mano and João Borges

Published by the Royal Society of Chemistry, www.rsc.org

oppositely charged bipolar amphiphiles,[2] polyelectrolyte multilayers,[3] and combinations thereof onto charged planar solid surfaces in the early 1990s.[4] Since then, the LbL technique has taken off and has quickly extended to the build-up of multifunctional multilayered assemblies encompassing an unprecedented array of materials (*e.g.* polymers, proteins, viruses, living cells, nucleic acids, nanoparticles, carbon nanotubes, clays) on virtually any kind of surface by resorting to a multitude of intermolecular interactions.[5] The fact that the assembly process can be performed at room temperature, in entirely aqueous solutions under mild conditions is a key advantage of the LbL technology, especially when aiming for biomedical and biotechnological applications.[6–8] Besides, the versatility endowed by the LbL technology is also unlocked by the panoply of deposition methods[9] and substrates[10] used to molecularly engineer the multilayer assemblies. Despite the tedious assembly process and the relatively large amount of materials needed for each deposition step, the dip-coating methodology is still the one that reunites more consensus to date due to the feasibility and easiness in coating flat, non-flat, and even substrates with more convoluted geometries. The LbL assembly process can be performed in any type of substrate, regardless of size, shape, surface chemistry, texture, and inanimate or animate nature, thus enabling shaping a diverse set of soft multilayered structures for addressing a wide variety of applications, including biomedical and biotechnological applications. In this chapter, we provide a comprehensive overview on the different types of substrates that have been conformally coated with an unprecedented choice of materials in a LbL fashion towards the preparation of a diverse set of multifunctional soft multilayered structures and devices, spanning from the zero-dimensional (0D) to the three-dimensional (3D), aimed for addressing a wide variety of biomedical applications. We anticipate that this chapter will spotlight the immeasurable possibilities and advantages imparted by the LbL technology, as well as fuel the academic and industrial communities with enlightened ideas for pushing up the development of innovative multilayered structures, exhibiting distinct composition, geometries, levels of complexity and (multi)functionalities, towards addressing practical biomedical applications.

18.2 Shaping Soft Structures Across Multiple Length Scales Using Inanimate Surfaces

The preparation of soft matter-based multidimensional nanostructures *via* template-assisted LbL assembly has gathered considerable attention in the biomedical and biotechnological fields, including as drug/gene/therapeutic carriers, bioreactors, intracellular trafficking devices, cell culture platforms, biomineralizable matrices, and tissue engineering scaffolds.[6–8] In this subchapter, emphasis will be given to the fabrication of 0D to 3D solid-core and hollow multilayered structures by LbL assembly of complementary single-component or multiple building blocks on a variety of inanimate templates.

18.2.1 0D Nanostructures

LbL-coating solid-core nanoparticles and hollow multilayered nanocapsules obtained after core template dissolution present themselves as highly attractive candidates for numerous biomedical applications owing to their straightforward synthesis, availability in different sizes, high biocompatibility, and enhanced surface-area-to-volume ratio. Herein, we will spotlight the most widely employed organic and inorganic cores to produce core–shell nanoparticles and hollow nanocapsules for biomedical applications.

18.2.1.1 Inorganic Core

18.2.1.1.1 Gold. Gold nanoparticles (AuNPs; 7–50 nm diameter) have been applied as templates for the production of electrostatically driven multilayered nanoparticles and hollow multilayered nanocapsules encompassing up to twenty oppositely-charged polyelectrolyte layers.[11] Grafting multifunctional molecules to polyelectrolytes is an attractive option to impart the developed layered structures with any desired multifunctionalities. For example, the fluorescence quenching effect of Au cores allows increasing the fluorescence intensity emitted from both core–shell nanoparticles and hollow nanocapsules while increasing the number of poly(allylamine hydrochloride) (PAH)/poly(sodium 4-styrenesulfonate) (PSS) bilayers assembled in-between the outer fluorescently labeled PAH layer and the Au core. These core–shell nanoparticles and hollow nanocapsules hold great promise in diagnostics, therapeutics, and theranostics applications, including as fluorescent sensors or photocontrollable delivery agents.[12] AuNPs are also suitable as nanodelivery vehicles of small interfering ribonucleic acid (siRNA) to cells, as demonstrated *via* dose-dependent knock-down of enhanced green fluorescent protein (eGFP) by CHO-K1/eGFP cells internalizing poly(ethyleneimine) (PEI)-functionalized AuNPs coated with PEI/siRNA multilayers.[13]

18.2.1.1.2 Iron Oxide. Multilayered iron oxide nanoparticles (IONPs; ~10 nm diameter) have been reported as suitable nanocarriers for the encapsulation and sustained release of model hydrophobic drugs. For instance, doxorubicin (DOX) loaded IONPs were orally administered for targeted DOX intestinal release by the inclusion of an outer milk protein casein layer, which was stable in acidic gastric conditions but degraded by the intestinal protease. Due to the magnetic core, the IONPs themselves and the guided drug release can be easily tracked *in vivo* by the generated magnetic resonance imaging (MRI) contrast enhancement.[14] Interestingly, the LbL technology can be used to improve the MRI contrast *via* the formation of multilayered clusters containing several IONPs, which yield a better contrast than single non-coated nanoparticles.[15] In turn, water-soluble magnetic luminescent nanoparticles were produced by coating iron oxide cores with cadmium selenide-based quantum dot (QD) layers,

spaced by PAH/PSS bilayers. The QD distribution and the number of bilayers allowed tailoring the photoluminescence intensity, turning these nanostructures into attractive platforms for the detection of water-soluble bioconjugates in immunoassays or bioseparation protocols.[16]

18.2.1.1.3 Silica. Antigen-loaded nanocarriers allow the direct targeting of labile vaccine antigens to antigen presenting cells (APCs), locally increasing cell proliferation and the immune response. In this regard, nonporous silica cores were used as templates to produce ovalbumin (OVA)-loaded thiolated poly(methacrylic acid) (PMA)/poly(vinylpyrrolidone) multilayered nanoparticles and hollow nanocapsules after silica template dissolution with hydrofluoric acid. Upon internalization by APCs, OVA-epitope presentation and activation of OVA-specific CD4 and CD8 T cells both *in vitro* and *in vivo* led to enhanced T cell proliferation when compared to OVA protein administered alone.[17] Moreover, silica nanospheres with a bimodal mesoporous structure (2–3 nm and 10–40 nm pores) have also been loaded with the enzyme catalase and successfully used for the effective encapsulation of the enzyme by LbL particle surface-coating with a multilayer nanoshell encompassing either oppositely-charged poly(diallyldimethylammonium chloride) (PDADMAC)/PSS or PDADMAC/silica nanoparticle hybrid multilayers. The combination of the bimodal mesoporous silica spheres and multilayered nanoshell not only protected the enzyme but also significantly improved its stability and maintained the enzymatic activity when compared with monomodal mesoporous silica spheres (2–3 nm pores) even upon exposure to enzyme-degrading substances, thus being a highly suitable nanocarrier for biocatalytic applications.[18]

18.2.1.1.4 Other. Given the importance of the outer-layer chemistry on the *in vivo* biological performance, the functionalization of carboxyl-modified QDs with a multilayer nanoshell comprising either oppositely-charged poly(L-lysine) (PLL)/dextran sulfate (DS) or PLL/hyaluronic acid (HA) bilayers was assessed for application in immunotherapeutic approaches to cancer therapy based on the enhanced permeation and retention (EPR) effect. In comparison with the uncoated and DS-ended QDs, the HA-ended QDs not only demonstrated an increased stability and lower liver accumulation, but also accumulation and clearance profiles in subcutaneously induced tumors in mice, being indicative of passive EPR-based targeting.[19]

Due to their antibacterial properties, silver nanoparticles (AgNPs) have gathered increasing attention. However, the low stability and inherent cytotoxicity extensively limit their biomedical applications. Tzanov and co-workers recently reported an attractive way to circumvent these issues by the electrostatic driven LbL decoration of AgNPs with oppositely-charged aminocellulose and acylase multilayers. This approach imparted the LbL-coated nanoparticles with enhanced antibacterial and antibiofilm activities without compromising cell viability.[20]

18.2.1.2 Organic Core

18.2.1.2.1 Polystyrene. Polystyrene (PS) cores are commonly employed to produce multilayered nanoparticles and hollow nanocapsules.[21] As an immunotherapeutic approach, the adsorption of A33 monoclonal antibody onto PAH/PSS multilayered nanoparticles and hollow nanocapsules enabled selective binding and internalization by A33 antigen-presenting colorectal carcinoma-derived cells. The cell binding specificity was tuned by varying the nanoparticle/nanocapsule size and outer polyelectrolyte layer.[22] Moreover, the release rate of rhodamine B from the multilayered nanocapsules composed of photocrosslinkable benzophenone modified-PAH/PSS was tuned by varying the degree of UV crosslinking and the number of bilayers.[23]

18.2.1.2.2 Other. The multilayer nanoshell composition also impacts the nanoparticle colloidal stability. A combination of PEI with either polyanions tripolyphosphate or DS multilayers on chitosan (CHT) nanoparticles showcased that the DS-coated nanoparticles (250 nm diameter) presented a higher stability, while both multilayered strategies enabled a pH-independent controlled release of nicotinic acid.[24] The development of a sandwich immunoassay for the detection of immunoglobulin G (IgG) consisted of coating microcrystalline fluorescein diacetate nanoparticles (~500 nm diameter) with PAH/PSS multilayers and subsequent adsorption of IgG antibodies. Following the nanoparticle immunoreaction with the substrate, the fluorescein diacetate core was dissolved by exposure to an organic solvent and converted into soluble fluorescein, where the emitted relative fluorescence intensity rivaled that of commercially available fluorescein isothiocyanate (FITC)-labeled IgG.[25]

18.2.2 1D Nanostructures

The development of 1D solid multilayered nanofibers and hollow multilayered nanotubes after template dissolution has been receiving increasing attention in biomedicine. Herein, we will focus on the role of porous and nonporous nanosized templates to assemble 1D multilayered nanofibers and hollow nanotubes.

18.2.2.1 Porous Nanosized Templates

Sacrificial membrane templates containing uniform and vertically-oriented nanometer-sized cylindrical pore arrays, such as track-etched polycarbonate (PC) and anodic aluminum oxide (AAO), have been employed to precisely fabricate 1D hollow nanotubular LbL nanoensembles after coating the inner pores with complementary molecules in a multilayered fashion and template liberation.[26–29] Caruso and co-workers reported the preparation of either polyelectrolyte or polyelectrolyte/AuNPs hybrid multilayered nanotubes onto PC membrane templates containing cylindrical pores of 400 nm in diameter, followed by template dissolution in dichloromethane (DCM).[26] Martin and

co-workers reported the covalent bonding-driven LbL assembly of protein-based nanotubes by alternate assembly of either glutaraldehyde (GA)/glucose oxidase (GOx) or GA/hemoglobin (Hb) multilayers onto 3-amino propylphosphonic acid functionalized nanoporous AAO template walls.[29] However, most of the nanotubes were broken during the template dissolution process. Hence, Komatsu and co-workers LbL-assembled electrostatic-driven multilayers comprising human serum albumin (HSA) and oppositely-charged synthetic polyelectrolytes (*e.g.* poly-L-arginine hydrochloride (PLA)) onto nanoporous PC templates to produce conformal and robust multilayered nanotubes in the form of a lyophilized powder after template dissolution and rapid freeze-drying of the extracted nanocylindrical cores (Figure 18.1A and B), as denoted by scanning electron microscopy (SEM) (Figure 18.1C and D).[30,31] The HSA-containing multilayered nanotubes not only retained their tubular structures but also denoted a high propensity to capture a series of molecules in their nanocylindrical inner walls, including DNA,[32] biotinylated nanoparticles (Figure 18.1E), enzymes,[30,31] and viruses,[33] among others.[34] An alternative nanotube quantitative collection method was also proposed by Jonas and co-workers based on adjuvant-assisted filtration.[35] Fully biocompatible and biodegradable nanotubes encompassing protein/lipid,[36] single-component protein,[37] and either wholly polypeptide[38] or marine polysaccharide[39] multilayers have been also prepared, thus extending their potential applicability in the biomedical field. More recently, Wang *et al.* made use of a PC membrane template exhibiting well-defined cone-shaped pore arrays with a diameter of 200 nm at the small opening and 800 nm at the big opening to develop $(PAH/PSS)_{10}$ multilayer tubular nanoswimmers functionalized with gold nanoshells on the inner walls.[40] Their ability to photomechanically perforate the membrane of a single-HeLa cancer cell was demonstrated aided by near-infrared light irradiation of the big opening pores enclosing the gold nanoshells. One can foresee the development of similar self-propelled nanoswimmers by resorting to fully biocompatible and biodegradable extracellular matrix (ECM)-derived nanosized multilayers, offering great prospects in a wide variety of biomedical and biotechnological applications, including as smart drug/gene/therapeutic nanoreservoirs.

18.2.2.2 Nonporous Nanosized Templates

High-aspect-ratio polymeric electrospun fiber mats with nanometer-size diameter and centimeter length have been produced by electrospinning and used as templates to produce multilayered nanofibers and even nanotubes, after core fiber template dissolution. These 1D nanostructures hold great promise for use in several biomedical applications, including in biosensing, separation, controlled drug delivery, and tissue engineering and regenerative medicine. In this regard, negatively charged electrospun cellulose acetate and PS nanofibrous mats, as well as glass fibers have been widely used as cylindrical templates to assemble a series of multilayered nanofibers and hollow multilayered nanotubes,[41–44] comprehending

A
D_p
Polycation
Protein
1) Alternate filtrations
PC template
D_p: 200, 400, 800 nm
PC-embedded
protein nanotubes
2) Removal of
surface layer
Air drying
PC/protein membrane
3) Dissolution of template
4) Freeze drying
Protein nanotubes
B
ca. 9 mm
Layer-by-Layer (LbL) structure
C
400 nm
D
400 nm
E
200 nm
200 nm

different combinations of functional complementary materials, after template removal *via* either chemical[42] or thermal treatment.[43] Müller *et al.* reported the successful and uniform LbL decoration of 400 nm diameter sulfonated PS nanofibers with electrostatic-driven $(PAH/PSS)_n$ multilayers after the treatment of the PS nanofibers with sulfuric acid to obtain a negatively charged surface.[42] Furthermore, the formation of conformal hollow polyelectrolyte multilayered nanotubes was revealed after template removal, denoting that the nanofiber's multilayered coating was kept intact. Besides, the preparation of nanotubes encompassing either electrostatic polyelectrolyte/AuNPs hybrid multilayers or non-electrostatic DNA oligonucleotide multilayers was also attempted. It was shown that the nanofiber's composition, length, and inner and outer (*i.e.* wall thickness) diameters could be precisely tailored by playing with the assembled materials, nanofiber template length, template diameter, and number of deposited layers, respectively.

18.2.3 2D Nanostructures

Since an early stage, LbL technology has been employed to coat a variety of flat non-patterned and patterned templates to produce 2D nanostructured multilayered thin films and thick and robust free-standing membranes with a wide variety of applications in the biomedical field.

18.2.3.1 Nanostructured Multilayered Thin Films

The fabrication of 2D multilayered nanostructures tightly bound to underlying substrates has received considerable attention in biomedical and biotechnological applications mainly due to their ability to encapsulate, protect, and spatiotemporally release on-demand a variety of bioactive molecules at a well-defined target site.[45] Herein, emphasis will be given to the fabrication of nanostructured multilayered thin films on flat non-patterned and patterned templates by resorting to a wide variety of ingredients.

Figure 18.1 (A) Schematic illustration of the template-assisted LbL assembly of protein-based multilayered nanotubes on track-etched nanoporous PC membrane template. (B) Schematic representation of (PLA/HSA)3 multilayered nanotube prepared using a 400 nm porous PC template. (C and D) SEM micrographs of the lyophilized powder (C) of the aqueous dispersion (D) of (PLA/HSA) multilayered nanotubes prepared using a 400 nm porous PC template, after freeze-drying *in vacuo*. (E) Transmission electron micrographs of (PLA/HSA)2PLA/poly-L-glutamic acid/Avidin multilayered nanotubes before (left) and after (right) the encapsulation of 100 nm biotinylated fluorescent nanoparticles (biotin-FNPs) and respective schematic illustration of the biotin-FNPs capture in the nanotubes.
Adapted from ref. 31 with permission from American Chemical Society, Copyright 2010.

18.2.3.1.1 Flat Non-patterned Templates

18.2.3.1.1.1 Glass ~~Substrates~~. Glass substrates have been one of the most widely reported templates ~~used~~ to prepare multilayered thin films. For instance, Criado-Gonzalez *et al.* reported the loading of sprayable $(ALG/CHT)_5$ functionalized PEI-modified glass substrate with tamoxifen, a well-known breast cancer drug, followed by the spraying-induced deposition of a distinct number of $(CHT/ALG)_n$ bilayers ($n = 5$, 10, and 20).[46] It was shown that the drug release profile could be modulated by playing with the number of bilayers, with the highest tamoxifen release being obtained for the lowest number of bilayers. Furthermore, the *in vitro* cellular assays revealed that the human breast cancer cell viability decreased upon exposure to tamoxifen-loaded multilayered assemblies.

18.2.3.1.1.2 Quartz ~~Substrates~~. Almost thirty years ago, Decher *et al.* successfully developed LbL multilayered assemblies encompassing oppositely-charged polyelectrolytes on quartz substrates as monitored by UV–vis spectroscopy and small angle X-ray scattering.[47] Since then, the development of multilayered thin films on quartz substrates has gained increasing attention. Yang and co-workers developed $(CHT/HA)_4/(CHT/HA\text{-}siRNA)_n$ ($n = 0$–15 bilayers) multilayered thin films on a quartz substrate *via* UV–vis spectroscopy, denoting the effective loading and sustained release of siRNA from the multilayered films up to nine siRNA-loaded bilayers.[48] This kind of surface-mediated non-viral platform holds great promise in the localized and sustained release of siRNA in mucosal tissues.

18.2.3.1.1.3 Silicon Wafer ~~Substrates~~. Silicon wafers have also been widely used as substrates to build-up multilayered nanoensembles for fulfilling biomedical purposes. Recently, Hong and co-workers reported the LbL build-up of biocompatible carboxymethyl cellulose (CMC)/CHT multilayered nanofilms on a silicon wafer and revealed that, by playing with the inner structure of the multilayered film, one can easily control and screen the loading and release profile of drugs according to their molecular weight (Figure 18.2I-A).[49] Moreover, the antibacterial and anti-inflammatory activity imparted by the CMC/CHT nanofilms turn them into highly suitable assemblies to coat ophthalmic silicone tubes to produce a multifunctional tube for the surgical treatment of nasolacrimal duct obstruction.[50]

18.2.3.1.1.4 Gold ~~Substrates~~. Gold substrates have been one of the most widely used substrates for the LbL deposition of multilayered thin films for biomedical applications owing to their bioinert properties. In this regard, Jayakumar *et al.* developed a biosensor-based LbL film with controllable 3D nanoarchitecture encompassing first-generation poly(amido amine) dendrimer (PAMAM)-functionalized reduced graphene oxide and AuNPs layers assembled onto a mercaptopropionic acid-functionalized gold substrate for the analysis of DNA hybridization at ultra-trace levels,

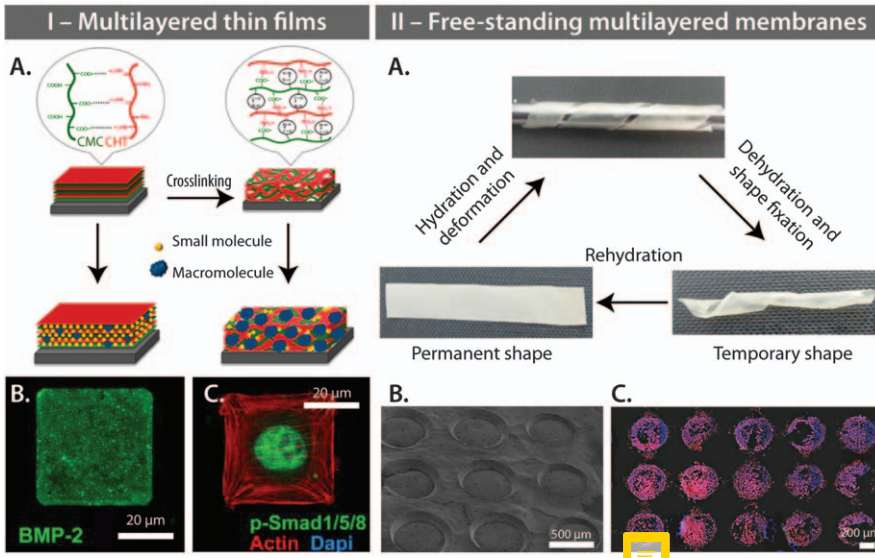

Figure 18.2 (I) (A) Schematic illustration of the cross-linking-induced structural change of the CMC/CHT multilayered films and its influence on the loading of drugs with different molecular weights. Adapted from ref. 49 with permission from American Chemical Society, Copyright 2017. (B) Confocal laser scanning microscopy micrograph of micropatterns of FN/BMP-2. (C) Immunofluorescence micrograph of C2C12 myoblasts after 4 h of culture on the surface of FN/BMP-2 micropatterns. (B and C) Adapted from ref. 56 with permission from Springer Nature, Copyright 2017. (II) (A) Shape memory behavior of (CHT/ALG)100 free-standing multilayered membranes induced by hydration. Reproduced from ref. 67 with permission from John Wiley & Sons, Copyright 2015 WILEY-VCH Verlag GmbH & Co. KGaA, Weinheim. (B) SEM and (C) DAPI/phalloidin fluorescence images at 7 days of culture of (CHT/ALG)100 free-standing multilayered membranes patterned with micro-wells. Adapted from ref. 69 with permission from Elsevier, Copyright 2017.

allowing the rapid diagnosis of genetic diseases.[51] Moreover, Borges *et al.* reported for the first time the LbL assembly of biocompatible supramolecular thin films encompassing ALG biopolymer and oppositely-charged self-assembling peptide amphiphile (K_3PA), revealing that the K_3PA-ended nanofibrous LbL films enhanced C2C12 myoblast cell functions.[52] However, the preparation of LbL films has not been limited to supramolecular interactions. Jerry and co-workers prepared smooth, homogeneous, and biocompatible LbL single component poly(ethylene glycol) (PEG) nanofilms on gold substrates by the sequential deposition of bifunctional and tetrafunctional PEG molecules *via* thiol/maleimide click chemistry, denoting great potential for biomedical purposes.[53]

18.2.3.1.1.5 Polystyrene ~~Substrates~~. Silva *et al.* developed non-crosslinked and genipin-crosslinked biocompatible $(CHT/ALG)_5$ multilayered thin films

on inert and hydrophobic PS substrates aiming to spotlight the key role of the nanocoating's surface chemistry on tailoring the human umbilical vein endothelial cell's (HUVECs) fate.[54] It was shown that the non-crosslinked nanofilms did not trigger cell adhesion owing to their low stiffness and high hydration level, whereas the crosslinked ones denoted an increase in stiffness and a more hydrophobic behavior while increasing the concentration of genipin, thus enhancing cell adhesion, spreading, and proliferation. Moreover, the deposition of an additional CHT/ALG bilayer on top of the crosslinked nanofilms led to a decrease in the adhesion, spreading, and proliferation of HUVECs to similar levels to those obtained on the non-crosslinked films, highlighting the key role of nanofilm surface properties in modulating cell–nanofilm interactions and cell functions.

18.2.3.1.2 Flat Patterned Templates. Besides flat smooth and non-patterned substrates, the versatility imparted by the LbL assembly technology has also been effectively applied to coat other types of flat surfaces, including rough, porous, and patterned substrates. Cho *et al.* developed (poly(β-amino ester)/OVA)$_{10}$ multilayered thin films in PC-based cylindrical porous membrane templates of various pore diameters to modulate the release kinetics of OVA, as well as suppress the initial burst release encountered in multilayered films assembled onto flat substrates without altering the film properties.[55] In another study, micropatterns of ~~fibronectin (~~FN~~)~~-bound ~~bone morphogenetic protein-2 (~~BMP-2~~)~~ were transferred into slightly crosslinked soft PLL/HA LbL films *via* microcontact printing promoting C2C12 myoblast adhesion (Figure 18.2I-B and C), as opposed to the FN/BMP-2-free non-cell adhesive PLL/HA multilayers.[56] The proposed micropatterns offer a promising route to investigate the mechanisms triggering BMP-2-mediated mechanotransduction or to explore other combinations of ECM proteins and growth factors aiming to recreate tissue-specific niches in *in vitro* microenvironments. Likewise, flat superhydrophobic PS surfaces were decorated with patterned wettable regions of modular size and shape for the build-up of LbL films encompassing different combinations of CHT and oppositely charged dopamine-modified HA (HA-DN) for a fast high-throughput screening.[57] *In situ* mechanical tests and *in vitro* cellular assays revealed that multilayered films containing a higher amount of catechol groups, *i.e.* CHT/HA-4DN denoted the highest adhesive strength and cell adhesion, with both parameters increasing while increasing the number of bilayers.

18.2.3.2 Nanostructured Free-standing Multilayered Membranes

Over the past two decades, the fabrication of robust, thick, and detachable multilayered films and innovative devices with intrinsic mechanical integrity and fine-tuned properties and functions at the nanoscale has gathered tremendous attention in numerous biomedical and biotechnological applications. Herein, we will spotlight the different strategies that have been employed to gently detach thick films from the underlying substrates,

thus producing self-sustained films, usually termed as free-standing multilayered membranes.

18.2.3.2.1 Flat Non-patterned Templates

18.2.3.2.1.1 Hydrophilic ~~Substrates~~. A typical approach to detach multilayered films from hydrophilic surfaces consists of the deposition of weak sacrificial layers on the underlying substrate prior to the multilayered film build-up. The release of the LbL films is subsequently carried out through the selective dissolution of the bottom sacrificial layers *via* solvent-assisted methodologies[58] or by specific triggering mechanisms, including pH variations, salt concentration, redox, or even light irradiation.[59–61] Both strategies have been successfully applied to develop free-standing membranes with envisioned drug delivery ability to be applied as drug releasing patches.[58,59] In particular, the pH-induced dissolution of the sacrificial layers has been widely used to break-up the hydrogen-bonding interactions between the pre-deposited layer and the substrate under mild conditions, thus avoiding the use of undesirable organic solvents.[61,62] In fact, when dealing with hydrogen-bonded multilayered assemblies, a pre-crosslinking treatment should be applied, before the pH triggering dissolution of the sacrificial layer, aiming to increase the chemical stability and mechanical strength of the further hydrogen bond-driven free-standing multilayered membranes.[62] Nevertheless, the pH-triggered release of multilayered assemblies may represent a harsh condition that can affect the original pristine bulk properties and the chemical stability of sensitive biological materials, including proteins and cells, jeopardizing the biological performance of the developed multilayered assemblies. One innovative and biologically friendly way to induce the detachment of pH- and ionic strength-stable multilayered films under mild conditions was recently proposed by Rubner and co-workers, who reported the assembly of biologically specific mucin/lectin multilayers capable of being completely disassembled from the underlying glass substrate, under physiological conditions, upon exposure to a competitive melibiose-based inhibitor sugar.[63] The released free-standing multilayered films were further attached to the cell surfaces as cell ''backpacks'', without any sign of cytotoxicity, denoting their intrinsic ability to be used as reservoirs for the effective loading and release of drugs.

18.2.3.2.1.2 Hydrophobic ~~Substrates~~. Taking advantage of the hydrophobic nature and low surface energy of polypropylene (PP) substrates, Hammond and co-workers firstly reported the concept of detachable multilayered films, *i.e.* free-standing films without the use of sacrificial layers.[64] Such substrates have also been used for assembling free-standing LbL membranes encompassing biological materials, including polysaccharides, nucleic acids, peptides, growth factors, and therapeutic agents without jeopardizing their chemical stability and biological activity. For instance, natural-based biopolymers have been combined with bioactive glass nanoparticles on PP substrates to produce nacre-inspired bioresorbable free-standing membranes for tackling periodontal diseases. The membranes can act both as a physical

barrier to protect the defect site and as a scaffold for triggering bone tissue regeneration.[65] Besides, biopolymer-based free-standing membranes imparted with adhesive catechol groups have been used as advanced bio-adhesive patches for wound healing.[66] In addition, the functional catechol moieties can be used as a crosslinking strategy to tune the mechanical strength of the free-standing membranes that would impact cellular attachment. Biopolymer-based free-standing membranes have also exhibited shape memory ability, undergoing reversible geometric transformation upon hydration or ionic crosslinking (Figure 18.2II-A).[67,68] These smart biomaterials hold great promise for being used as implantable devices, being inserted in the defect site (*e.g.* bone or cartilage defects) through a small incision in a temporary shape and subsequently reaching a permanent shape after a certain hydration level is achieved.

18.2.3.2.2 Flat Patterned Templates. Patterned hydrophobic and low surface energy substrates have been widely used for the fabrication of free-standing patterned multilayered membranes to modulate cell functions. Polydimethylsiloxane substrates with patterned geometrical features were used to produce biopolymeric free-standing multilayered membranes with a tuned array of micro-wells where osteoblast-like cells tended to colonize preferentially (Figure 18.2II-B and C).[69] Such well-defined micro-pore arrays could act as micro-reservoirs for the delivery of bioactive agents or as cell carrier patches for regenerative medicine. While microscale geometrical motifs are known to influence cell adhesion, migration, and organization, nanoscale topographical features have been employed to regulate cell proliferation, differentiation, alignment, or gene expression. Sousa *et al.* produced nanogrooved multilayered films by LbL coating nanopatterned PC templates denoting nanogrooved features.[70] These nanotopographical features played a pivotal role in modulating C2C12 myoblast cell alignment along the nanopattern direction and in triggering their differentiation into myotubes, thus holding great promise in muscle tissue regeneration. This approach could be adapted to other cell types that respond to topographical features, including neuronal or endothelial cells, to prompt the regeneration of nerves or blood vessels.

18.2.4 3D Structures

Beyond the preparation of 0D, 1D, and 2D LbL architectures, LbL technology has shown remarkable potential to coat more convoluted 3D surfaces, including colloidal particles, tube-like or cylindrical, and porous and interconnected structures, demonstrating that LbL technology can coat virtually any kind of surface and find widespread use in many biomedical applications.

18.2.4.1 Micro/Macro-particles and Hollow Capsules

LbL technology can be scaled-up to the third dimension simply by alternatively assembling multilayers onto 3D substrates. The current subchapter will focus on the fabrication of micro- and macro-sized core–shell colloidal

particles and hollow LbL structures by resorting to either a variety of organic or inorganic core templates and LbL ingredients for addressing a wide variety of biomedical applications.

18.2.4.1.1 Inorganic Templates. The LbL assembly of complementary materials onto biocompatible micro-sized inorganic templates into core–shell microparticles and further hollow multilayered microcapsules after core template dissolution has been widely reported.[71–74] For instance, Sukhorukov and co-workers reported the preparation of biocompatible hollow multilayered microcapsules by LbL coating calcium carbonate ($CaCO_3$) microcores with either electrostatic-driven ALG/PLA or DS/PLA multilayered shells, followed by core template dissolution with ethylenediaminetetraacetic acid (EDTA).[75] The encapsulation of the model protein bovine serum albumin (BSA) during the synthesis of the $CaCO_3$ microcores (*i.e.* ''pre-loading'') and in the preformed hollow multilayered microcapsules (*i.e.* ''post-loading'') revealed that the protein's release kinetics was faster in the ''post-loaded'' microcapsules than in the ''pre-loaded'' ones, as well as for the multilayered shells encompassing the lowest number of bilayers. More recently, Mano and co-workers reported the fabrication of biomimetic hollow microcapsules comprising either CHT/elastin-like recombinamer (ELR)[72] or CHT/ALG multilayered shells[71] for intracellular delivery and enhanced cellular internalization, respectively. Silk-on-silk microcapsules with the desired permeability were also templated onto silica microparticles for being used in sustained drug delivery.[74] Another way of controlling the release of encapsulated loads from inorganic colloidal microcores concerns the development of stimuli-responsive multilayered shells. These include light- and pH-responsive DNA-based microcapsules templated on PAH-functionalized $CaCO_3$ microcores enclosing six layers of photocleavable DNA multilayered nanoshells (Figure 18.3I-A).[76] When exposed to UV light irradiation ($\lambda = 365$ nm), the all-DNA microcapsules disrupted and released the respective content due to the cleavage of the *o*-nitrobenzyl linkers that formed *o*-nitrosobenzophenone units. Likewise, pH-responsive DNA-based microcapsules were prepared consisting of DNA bridging units that were reconfigured at acidic pH values into i-motif structures. The exposure to a pH 5 environment resulted in the dissociation of the DNA multilayered shell, promoting the release of the encapsulated loads.

18.2.4.1.2 Organic Templates. Biocompatible and biodegradable CHT microparticles prepared by an aerodynamically-assisted jetting technique and further coated in a stepwise LbL fashion with biopolymeric materials have been used for the encapsulation and sustained release of a hydrophilic local anesthetic drug.[77] For that, the deposition of up to three poly(D-lactic acid)/poly(L-lactic acid) (PDLA/PLLA) bilayers onto CHT microparticles was attempted *via* stereocomplexation. The presence of the hydrophobic stereocomplex multilayered nanoshell decreased the porosity of the microparticle surface, slowing down the release kinetics of the model drug procaine hydrochloride. Such core–shell microparticles offer a promising route for the

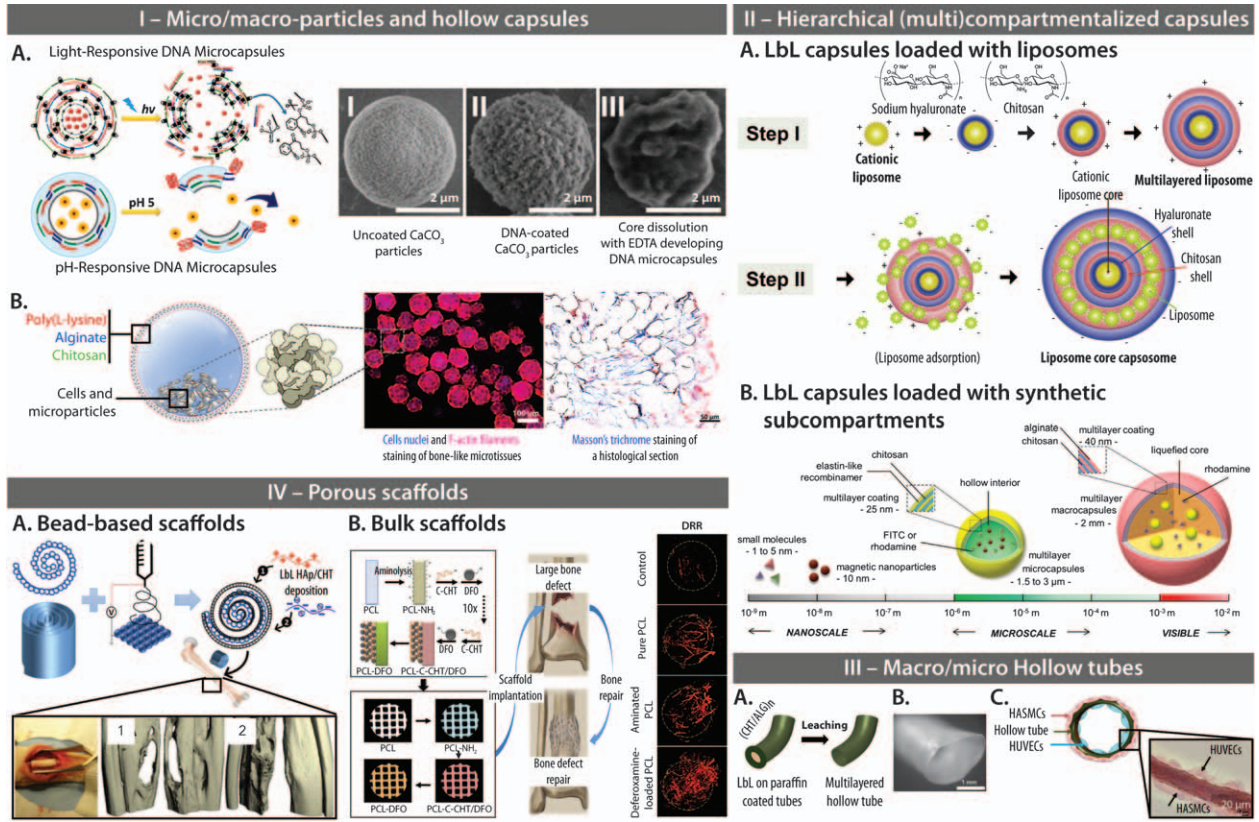
I – Micro/macro-particles and hollow capsules
A. Light-Responsive DNA Microcapsules
hv
pH 5
pH-Responsive DNA Microcapsules
I
II
III
2 µm
Uncoated CaCO3 particles
DNA-coated CaCO3 particles
Core dissolution with EDTA developing DNA microcapsules
B.
Poly(L-lysine)
Alginate
Chitosan
Cells and microparticles
Cells nuclei and F-actin filaments staining of bone-like microtissues
Masson's trichrome staining of a histological section
II – Hierarchical (multi)compartmentalized capsules
A. LbL capsules loaded with liposomes
Step I
Sodium hyaluronate
Chitosan
Cationic liposome
Cationic liposome core
Multilayered liposome
Step II
Hyaluronate shell
Chitosan shell
Liposome
(Liposome adsorption)
Liposome core capsosome
B. LbL capsules loaded with synthetic subcompartments
alginate chitosan
multilayer coating - 40 nm -
liquefied core
rhodamine
chitosan
elastin-like recombinamer
multilayer coating - 25 nm -
hollow interior
multilayer macrocapsules - 2 mm -
FITC or rhodamine
small molecules - 1 to 5 nm -
magnetic nanoparticles - 10 nm -
multilayer microcapsules - 1.5 to 3 µm -
NANOSCALE
MICROSCALE
VISIBLE
IV – Porous scaffolds
A. Bead-based scaffolds
LbL HAp/CHT deposition
B. Bulk scaffolds
Aminolysis
C-CHT
DFO
PCL
PCL-NH2
10x
PCL-DFO
PCL-C-CHT/DFO
Scaffold implantation
Large bone defect
Bone repair
Bone defect repair
DRR
Control
Pure PCL
Aminated PCL
Deferoxamine-loaded PCL
III – Macro/micro Hollow tubes
A.
(CHT/ALG)n
Leaching
LbL on paraffin coated tubes
Multilayered hollow tube
B.
C.
HASMCs
Hollow tube
HUVECs
HUVECs
HASMCs
20 µm

development of anesthetic release systems. Organic core–shell microcores have also been envisioned as cell carriers for tissue engineering applications. In this regard, Mano and co-workers encapsulated human osteoblasts and adipose-derived stem cells (hASCs) in liquefied ALG microcapsules encompassing a ten-layered PLL/ALG/CHT membrane to be used as mini-reactors for the *in vitro* production of bone-like microtissues (Figure 18.3I-B).[78] Besides, LbL technology has been proposed to create spherical synthetic carriers that resemble the structural features of red blood cells (RBCs). Mitragotri and co-workers sequentially assembled nine layers of either PAH/BSA or Hb/BSA onto the surface of biocompatible poly(lactic acid-*co*-glycolide) (PLGA) microparticles, followed by chemically crosslinking the multilayered shell with GA prior to the core template dissolution.[79]

Figure 18.3 (I) (A) Schematic illustration of light- and pH-induced DNA microcapsules. SEM micrographs corresponding to (I) bare $CaCO_3$ microparticles, (II) DNA-coated $CaCO_3$ microparticles, and (III) DNA microcapsules. Adapted from ref. 76 with permission from American Chemical Society, Copyright 2016. (B) Liquefied and multilayered microcapsules encapsulating stem cells and microparticles. The fluorescence microscopy image (left image) represents bone-like microtissues and the corresponding histological section staining collagen in blue (right image). Adapted from ref. 78 with permission from IOP Publishing, Copyright 2019. (II) (A) Schematic representation of the formation of capsosomes composed by a cationic liposome core surrounded by a HA/CHT LbL membrane coated with smaller sized liposomes encapsulated in a single HA/CHT bilayer. Reproduced from ref. 86 with permission from Elsevier, Copyright 2016. (B) Schematic illustration denoting the hierarchical organization of multifunctional multicompartmentalized capsules: liquefied ALG beads composed by (CHT/ALG)3 LbL nanoshells encapsulating molecular compounds and $CaCO_3$-templated multilayered microcapsules delimited by (CHT/ELR)3 LbL nanoshells and loaded with other types of molecular compounds and magnetic nanoparticles. Reproduced from ref. 92 with permission from American Chemical Society, Copyright 2013. (III) (A) Schematic representation of the (ALG/CHT)100 macro hollow tube preparation. (B) Optical microscopy image of (ALG/CHT)100 macro hollow tube in dry state. (C) Histological cross-section of (ALG/CHT)100 macro hollow tubes seeded with HUVECs and HASMCs after 7 days of culture. (A and C) Adapted from ref. 96 with permission from American Chemical Society, Copyright 2016. (B) Reproduced from ref. 95 with permission from John Wiley & Sons, Copyright 2013 WILEY-VCH Verlag GmbH & Co. KGaA, Weinheim. (IV) (A) Schematic representation of HAp/CHT-coated spiral PLGA scaffold production. Scaffold implantation in rabbit ulnar defect with corresponding micro-CT reconstructions at 10 weeks post-implantation for (1) cylindrical and (2) spiral scaffolds. Adapted from ref. 99 with permission from American Chemical Society, Copyright 2018. (B) Schematic representation of the preparation of C-CHT/DFO multilayers on PCL scaffolds (left upper panel) and four distinct scaffolds used in the animal study (left lower panel). Digital reconstructed radiographs after micro-CT scanning of newly formed vascular structure 2 weeks after scaffold insertion in the defect site for the four distinct scaffolds (right panel). Adapted from ref. 108 with permission from Elsevier, Copyright 2019.

The shape, flexibility, and size of the synthetic RBC-shaped PLGA template microparticles were shown to be reminiscent of natural RBCs, with high oxygen binding levels, even after 1 week, thus mimicking the natural function of the native cells. These synthetic carriers were denoted as excellent candidates for the treatment of thrombosis, simply by loading them with anti-coagulant heparin, or even for medical imaging, through the incorporation of IONPs as contrast agents for MRI.

18.2.4.2 Hierarchical (Multi)Compartmentalized Capsules

Living systems have served as inspiration for the development of engineered systems with confined and multiple spatiotemporal metabolic reactions with high accuracy and specificity.[80] Although considerable progress has been made to date in developing single compartment systems, ranging from liposomes and cellosomes (yeast cells surrounded by a polymer membrane) to polymersomes (polymer-based liposomes fabricated by the controlled self-assembly of amphiphilic block copolymers) and LbL capsules, the construction of highly complex multicompartmentalized systems as cell-inspired synthetic analogs has proven to be challenging. Several approaches, including multistep emulsification,[81] microfluidics,[82] and LbL assembly,[83] have been employed to engineer multicompartmentalized systems that could be employed for therapeutic cell mimicry *via* the encapsulation and/or conversion of biologically active materials. Different subcompartmentalized assemblies have been reported, namely in the form of vesosomes (liposomes-in-liposomes), polymersomes-in-polymersomes, capsosomes (liposomes-in-polymer capsules), cubosomes (highly stable nanoparticles formed from the lipid cubic phase and stabilized by a polymer-based outer corona), multicompartment microparticles, and subcompartmentalized polymer capsules. The current subchapter will focus on multicompartmentalized systems developed using the LbL technique for at least one of its components.

18.2.4.2.1 LbL Capsules Loaded with Liposomes. Capsosomes, fabricated *via* the alternate deposition of polymer and liposome layers onto a sacrificial colloidal template, have demonstrated their effectiveness as microreactors[84] and drug delivery vehicles.[85] A polymer precursor layer is first absorbed onto the template, followed by the deposition of a liposome to form the initial polymer/liposome bilayer. After the adsorption of the desired number of bilayers, a polymer capping layer is then absorbed followed by the LbL assembly of the membrane of the polymer carrier capsule and subsequent dissolution of the particle template. The colloidal template is mainly composed by a silica core, although other alternatives have recently been explored, such as a liposomal core, which eliminates the need for core dissolution (Figure 18.3II-A).[86] Different polymers, namely PLL, cholesterol-modified PLL, poly(methacrylic acid)-*co*-cholesteryl methacrylate, or a combination thereof, have shown to allow for multilayer formation atop of liposomes without jeopardizing their own structural integrity.[87] Electrostatic

interactions alone can be limiting in the selection of the liposomes and polymers that can be assembled to produce capsosomes due to restrictions in the affinity between the liposomes and the precursor and/or capping polymer layers. In particular, cholesterol provides a widely applicable noncovalent anchor between polymer layers and liposomes.[88,89] The co-encapsulation of multiple enzymes and/or small molecules requires an understanding of the size-dependent retention of different cargoes in capsosomes, especially during their assembly. Although several studies have been reported on cargo encapsulation and pH properties in liposomes, there are different aspects that ought to be considered in the development of capsosomes, namely the effects assigned to the immobilization of liposomes onto polymer-coated silica particle surfaces and environmental pH changes during the assembly process. The cargo retention and pH changes within the liposomal counterpart can be simultaneously monitored using pH-sensitive fluorescent dyes.[87] The presence of liposomes allows fine-tuning of the permeability of capsosomes using temperature stimulus since their lipidic membrane enables the combination of different lipid compositions and, consequently, different phase transition temperatures.[90]

18.2.4.2.2 LbL Capsules Loaded with Synthetic Subcompartments. Multicompartmentalized systems relying exclusively on the LbL methodology are scarce in the literature. The strategy relies on the presence of a multilayered capsule enveloping several smaller multilayered capsules, and it has been suggested for vaccination purposes as "self-exploding" systems that release the entrapped LbL microcapsules,[91] or as a proof-of-concept nano-to-macro system triggered by temperature or magnetic stimuli (Figure 18.3II-B).[92] The majority of the reported multicompartmentalized polymeric capsules rely on a polymer capsule with concentric independently-loaded compartments prepared by the co-precipitation method employing hard, inorganic sacrificial templates, such as $CaCO_3$,[93] silica,[94] or hybrid all-in-water emulsion droplets.[81] Alternatively, LbL capsules have been successfully combined with polymersomes. Polymersomes present higher flexibility, tunable permeability, higher mechanical and colloidal stability, and enhanced durability compared to liposomes. Appelhans and co-workers reported the development of LbL capsules surface-functionalized with PEG and encapsulating adamantly-functionalized polymersomes with metabolism mimicry of cell mimics, demonstrated by performing enzymatic cascade and competitive reactions in diffusion-controlled metabolite trafficking.[83]

18.2.4.3 Micro/Macro-hollow Tubes

LbL technology has also been employed to engineer hollow tube-shaped multilayered devices for tackling vascular diseases. In an attempt to develop blood vessel substitutes, Silva *et al.* constructed self-sustained multilayered hollow macro-tubes through the LbL build-up of ALG/CHT multilayers onto sacrificial paraffin-coated glass tubes followed by core template leaching

with DCM (Figure 18.3III-A and B).[95,96] Subsequently, tubes were crosslinked with genipin to increase the mechanical properties and decrease the water uptake and further functionalized with FN to enhance the cell adhesiveness of the multilayers. The developed hollow tubes were successfully co-cultured with HUVECs and human aortic smooth muscle cells (HASMCs) on the inner and outer sides of the tubes (Figure 18.3III-C), respectively, mimicking native blood vessels.[96] More recently, Colino *et al.* reported the LbL assembly of ELRs onto a metal mesh-like tube for developing free-standing membrane-coated stents for the treatment of coronary artery disease.[97] The ELR-membrane coated coronary stent not only exhibited mechanical stability upon exposure to arterial flow and pressure conditions, but also denoted the intrinsic ability to support the formation of a confluent endothelial layer, thus holding great promising to seal aneurysms or arterial perforations and successfully healing after stent implantation.

18.2.4.4 Porous Scaffolds

LbL technology is an attractive technique to tailor the surface properties, improve the mechanical properties, or modify the scaffold porosity and interconnectivity. This technology can be applied to either bulk scaffold coating developed in a top-down strategy or for bottom-up scaffold production *via* the aggregation and/or envelopment of unitary blocks.

18.2.4.4.1 Bead-based Scaffold. Mechanically robust 3D porous scaffolds have been prepared by combining poly(acrylic acid) (PAA)-grafted PLLA microspheres with the stepwise LbL assembly of either PAA/PAH or PAA/polyacrylamide multilayers onto the microsphere's surface, which maintained their structure through electrostatic or hydrogen-bonding interactions, respectively. Scaffolds could be rendered electrically conductive by the incorporation of a final graphene oxide or IONP layer.[98] Alternatively, spiral microparticle-based scaffolds were produced *via* roll-up of a monolayer of sintered PLGA microparticles with deposited PLGA nanofibers, which was further LbL coated with ~~hydroxyapatite (~~HAp~~)~~/CHT multilayers for the controlled release of calcium.[99] In a rabbit bone defect model, the spiral scaffolds improved the bone formation when compared to their cylindrical counterpart, likely due to a facilitated cell infiltration (Figure 18.3IV-A). Sher *et al.* reported the perfusion-based LbL deposition of ALG/CHT multilayers on softer calcium crosslinked cell-laden ALG-based structures to produce 3D self-sustaining liquefied scaffolds *via* mild calcium chelation, thus ensuring cell survival.[100,101] Upon multilayer build-up on packed ALG microbeads or reeled fibers, the subsequent chelation of the ALG template led to the formation of a liquefied interconnected environment for cells to proliferate freely. Cells themselves and the deposited ECM have also been applied as aggregation mediators of PLL/CHT/ALG multilayered microcapsules having an outer layer encompassing ALG functionalized with the bioactive cell adhesion motif arginine–glycine–aspartic acid (RGD).[102]

18.2.4.4.2 Bulk Scaffold

18.2.4.4.2.1 Electrospinning. The LbL coating of porous nanofibrous structures produced by electrospinning constitutes a promising strategy for the development of biologically relevant structures to be used in multiple biomedical applications. Hu *et al.* reported that the LbL deposition of an increasing number of oppositely-charged quaternized chitin/silk fibroin (SF) bilayers onto ~~polycaprolactone (~~PCL~~)~~/SF electrospun scaffolds allowed tailoring the mechanical properties of the scaffolds and enhancing their antibacterial properties.[103] Although the coating did not significantly increase the wound healing rates in rat full-thickness cutaneous defects, it enhanced the revascularization and led to the formation of hair follicles. Furthermore, the surface functionalization of electrospun PCL scaffolds with multilayers comprehending single-component SF further decorated with heparin disaccharide triggered the non-covalent binding of interleukin-4 in a murine subcutaneous implantation model, with the intrinsic capacity to tailor macrophage polarization. The functionalized scaffold promoted host cell infiltration and integration into the surrounding tissue, while reducing the formation of foreign body giant cells and fibrous tissue.[104] Besides, biodegradable PLGA-based electrospun microfiber scaffolds were functionalized with CHT/ALG nanolayers to promote the immobilization and subsequent controlled release of plasmid DNA (pDNA)/dendrimer complexes over time, while protecting the pDNA degradation. The functionalization with BMP-2 codifying pDNA not only promoted the adhesion and growth of human mesenchymal stem cells (MSCs), but also triggered gene transfection and induced osteogenic differentiation.[105] An advantage of the LbL technique is its application for the selective positioning of bioactive molecules between layers, which will be sequentially exposed upon degradation of the outer layers. Hence, osteoconductive PLGA/nano-HAp electrospun scaffolds have been coated with PSS/PAH multilayers grafted with distinct biofunctional peptide sequences along the multilayer build-up to direct bone marrow-derived MSCs adhesion and proliferation, induce osteogenesis, and ultimately promote matrix mineralization, with promising results in a rat calvarial model.[106]

18.2.4.4.2.2 Rapid Prototyping. Rapid prototyping is a promising technique to quickly fabricate 3D structures, which may be combined with LbL technology to produce customized micro/macro-scaffolds with precisely tailored properties and functions for biomedical purposes. Oliveira *et al.* reported the preparation of PCL macro-scaffolds functionalized with nanostructured multilayers encompassing human platelet lysate (PL) and marine-origin polysaccharides. Upon the LbL assembly process, the hierarchical scaffolds were freeze-dried to shape the PL-based LbL assemblies into nanofibrillar structures to direct the osteogenic differentiation of hASCs into osteoblasts.[107] More recently, Yan *et al.* also functionalized 3D porous aminated PCL scaffolds with ~~carboxymethyl~~ ~~CHT~~ ~~(~~C-CHT~~)~~/

deferoxamine (DFO) multilayers to stimulate the sustained release of DFO.[108] DFO is an iron chelator that functions as a hypoxia mimic compound under normoxia condition and renders similar outcomes by activating hypoxia inducible factor 1-alpha (HIF1-α), which modulates the expression of angiogenic and osteogenic related genes. Accordingly, both angiogenesis and osteogenesis were induced in a rat femur defect mode for the scaffolds presenting ten C-CHT/DFO bilayers (Figure 18.3IV-B).

18.2.4.4.2.3 Other. Scaffolds produced by alternative methods may also be functionalized *via* LbL to promote the loading of bioactive molecules. The LbL deposition of HA/CHT multilayers onto PEI-functionalized porous biphasic calcium phosphate scaffolds produced *via* hydrogen peroxide foaming was shown to sustain the loading of calcitriol at lower concentrations.[109] Calcitriol reportedly activates the calcium sensing receptor, a key modulator of osteogenic differentiation, which led to an enhanced regeneration of a critical-size rat calvarial bone defect model. Alternatively, dual drug-loaded PLGA microparticles were immobilized on porous HAp scaffolds produced *via* sol–gel and sugar particle leaching.[110] Prior to immobilization, osteogenic growth peptide-loaded microparticles were LbL coated with CHT/HA multilayers containing a central BMP-2/heparin bilayer. The system induced an increased expression of osteogenic-related genes in seeded human bone marrow stem cells *in vitro* and directed ectopic bone formation and vascularization *in vivo*.

The LbL methodology has the intrinsic capacity to deliver a multitude of functionalities. For instance, porous biocompatible polyurethane scaffolds coated with oppositely-charged methylene blue-loaded CHT and fluorescein sodium-loaded graphene oxide hybrid multilayers demonstrated a dual pH-dependent release of multiple therapeutic agents.[111] Due to the energy conversion of graphene oxide into heat upon NIR light absorption, the potential application in photothermal cancer therapy may be unveiled. Moreover, antimicrobial activity could also be conferred by alternatively loading CHT with AuNPs. On spiral titanium scaffolds, LbL pulse electrodeposition of polypyrrole–polydopamine nanoparticles and HAp nanoparticles synthesized *via* co-electropolymerization conferred seeded cells with protection against damage by reactive oxygen species due to the redox behavior of the electroactive nanoparticles. The synergistic activity of the electrical stimulation and the presence of HAp enhanced bone marrow stromal cells osteogenic differentiation *in vitro*, while an improved new bone formation was observed *in vivo* in a rabbit injury model.[112]

18.3 Shaping Soft Structures Across Multiple Length Scales Using Dynamic and Animate Surfaces

In the past few years, considerable efforts have been made within the LbL community to functionalize dynamic and animate surfaces, including living cells. Since the LbL assembly process can be performed in aqueous media

under mild conditions, it has become a very appealing tool for pursuing biomedical strategies.[113] The conventional electrostatic-driven LbL technology has been widely applied to create nanosized multilayer films onto the surface of cells by firstly functionalizing the negatively charged cell membrane surface with a cationic polymer, followed by the multilayer build-up with alternating oppositely charged polymers. This powerful technology can protect the cells against numerous foreign aggressions, thus quickly expanding to coat the surface of a vast array of living cells,[114] including bacteria,[115] yeasts,[116] stem cells,[117] tumor cells,[118] and islet cells.[119,120] In this subchapter, two different templates will be described for LbL cell-surface functionalization: single-cells and cell aggregates.

18.3.1 Coating of Single Cells

Due to the challenges experienced during the gastrointestinal transit, such as the extreme acidic pH and the presence of bile salts, cell viability is significantly reduced, thus limiting the clinical applications of probiotics.[121] As such, the encapsulation of probiotic microbes in LbL assemblies has been widely used to protect probiotics from the gastrointestinal tract's environment. For instance, Anselmo *et al.* sequentially encapsulated the probiotic strain *Bacillus coagulans* (BC) in CHT/ALG bilayers to improve their delivery *in vivo* (Figure 18.4I-A).[115] After the probiotic delivery *via* oral gavage, it was shown that the LbL protective coating not only significantly enhanced the BC viability, but also facilitated both the probiotic mucoadhesion and growth on the porcine intestine model surface when compared to plain-BC. In an attempt to treat myocardial infarction by minimally invasive procedures, Liu *et al.* encapsulated MSCs in a thin, three-layered vascular endothelial growth factor (VEGF)-loaded gelatin (G)/ALG multilayered shell to improve angiogenesis and cardiac function (Figure 18.4I-B).[117] The *in vitro* studies denoted that the proposed delivery system induced a sustained release of VEGF and tropism to stromal cell-derived factor-1, which is responsible for the recruitment of MSCs. The *in vivo* assays demonstrated that the delivery of VEGF-encapsulated MSCs *via* the tail vein enhanced cardiac function, perfused the infarct area and promoted angiogenesis.

The LbL assembly technology can also be used to enhance and modulate host immune responses, aiming for cell transplantation strategies. In this regard, the LbL encapsulation of living Bacille–Calmette–Guérin (BCG) mycobacteria with a nanocoating encompassing alternate layers of oppositely-charged CHT and microbial double-stranded RNA mimetic polyinosinic–polycytidylic acid (poly(I:C)) was proposed as an efficient strategy to co-deliver the poly(I:C) immunostimulating agent along BCG and to enhance BCG's immunogenicity, inducing a stronger and long-term protective immune response against adult pulmonary tuberculosis (Figure 18.4I-C).[122] It was shown that the multilayer coating enhanced the macrophage production of pro-inflammatory factors, including nitric oxide and cytokine production when compared to uncoated BCG.

I - Coating of single cells
II - Coating of cell aggregates
A.
Bacteria
Chitosan Layer
Alginate Layer
Repeat
(CHI/ALG)3
(i) Plain
(ii) LbL-(CHI/ALG)2
1.5 cm
B.
Perfused infarct area after 4 weeks post-myocardium infarction
Self-assembly
Alginate-Gelatin (load VEGF)
VEGF
MSCs
Homing
MSCs load VEGF homing MI promotes angiogenesis
Perfused myocardium (%)
LbL-MSCs
Control-MSCs
VEGF group
C.
BCG
Chitosan
p(HVI:Cl)
BCG/Chi/p(HC)
1x Repeat
(i)
(ii)
100 nm
30 nm
A.
PEM Film Growth
cell surface
Alginate
PLL-g-PEG
pancreatic islet
(i)
(ii)
10 μm
50 μm
B.
GA
MDT
PAMAM
ALGINATE
PAMAM Solution
Buffer Wash (3x)
Alg-HyPEG-N3 Solution
Repeat Layering
C.
FN
Gelatin
1) Layer-by-layer assembly of FN and gelatin on cell surface
first cell monolayer
first cell monolayer coated with nano-ECM films
2) Seeding and adhesion of second cell
second cell
3) Repeating processes (1) and (2)
3D multilayer
Bilayer
12.8 μm
6.5 μm

18.3.2 Coating of Cell Aggregates

The electrostatic interaction between oppositely-charged polyelectrolytes is often used to encapsulate cells to replace dysfunctional tissues or organs. However, positively charged polyelectrolytes generally elicit cytotoxic effects by transposing the cell membrane and accumulating intracellularly, triggering the formation of nanosized cell membrane pores, which may result in cell death. Having this in mind, Chaikof and co-workers synthesized a library of cytocompatible PLL-*grafted*-PEG (PLL-*g*-PEG) copolymers aiming to reduce the cytotoxicity of PLL upon deposition onto the islet cell membrane surface for pancreatic islet transplantation strategies.[119] PLL-*g*-PEG copolymers reduced the cell membrane disruption while simultaneously facilitating the deposition of oppositely-charged polyelectrolytes on the cell surfaces, denoting the viability and functionality of the proposed approach (Figure 18.4II-A). Besides, the successful encapsulation of living pancreatic islets was also confirmed *via* non-ionic LbL assembly using poly(*N*-vinylpyrrolidone) (PVPON) and natural polyphenol tannic acid (TA).[120]

Figure 18.4 (I) (A) Schem tic illustration of CHT/ALG coating on probiotic strain BC. Representative TMS images of (i) plain-BC and (ii) LbL-BC 1 h after oral gavage. Adapted from ref. 115 with permission from John Wiley & Sons, Copyright 2016 WILEY-VCH Verlag GmbH & Co. KGaA, Weinheim. (B) Schematic illustration of VEGF-loaded MSCs coated with G/ALG multilayers. *In vivo* micro-CT shows the perfused infarct area in (i) untreated mice, (ii) LbL-MSCs group, (iii) control-MSCs group, and (iv) VEGF group after 4 weeks post-myocardium infarction. (v) Border zone of the myocardium in the different groups. Adapted from ref. 117 with permission from Elsevier, Copyright 2017. (C) Representation of the LbL coating of live BCG with CHT/poly(I:C) bilayers. TEM micrographs of (CHT/poly(I:C))2 coated BCG: (i) Transverse section showing a two double-layer nanocoating on the bacterial surface (arrows), (ii) high magnification image showing that the nanocoating (arrows) lies on top of the electron-lucent capsule-like matrix (asterisks). Adapted from ref. 122 with permission from Elsevier, Copyright 2016. (II) (A) Schematic illustration of the pancreatic islets surface functionalized with PLL-*g*-PEG/ALG multilayered films. (i) Cell membrane is crossed by FITC-labeled PLL, whereas (ii) AlexaFlour488-labeled P12Pn[Dc] copolymers remain extracellular and adsorb to cell surfaces. Adapted from ref. 119 with permission from American Chemical Society, Copyright 2011. (B) Schematic illustration of the LbL pancreatic islet surface functionalization with PAMAM functionalized with MDT, SIL, and GA, and N3-functionalized hyperbranched ALG *via* covalent bonds. (i) Immunohistochemistry imaging of insulin (green), f-actin (red), and nuclei (blue) of four-layer coated islets. Adapted from ref. 123 with permission from American Chemical Society, Copyright 2020. (C) Schematic illustration of the fabrication of 3D cellular multilayers by LbL coating L929 fibroblast cell surfaces with FN/G multilayered nanofilms. (i and ii) 3D reconstructed CLSM cross-section images of bilayered human umbilical artery smooth-muscle cells and HUVECs with (i) or without (ii) seven-step-assembled FN/G nanofilms. Adapted from ref. 124 with permission from John Wiley & Sons, Copyright 2007 WILEY-VCH Verlag GmbH & Co. KGaA, Weinheim.

The hydrogen-bonded PVPON/TA nanocoating did not affect islet viability and denoted immunomodulatory properties by suppressing Th1 pro-inflammatory cytokine release. More recently, an alternative approach to generate uniform and stable nanocoatings on pancreatic islets was proposed by Gattás-Asfura *et al.*, who reported the functionalization of cell surfaces with oppositely-charged hyperbranched polymers enclosing complementary Staudinger ligation groups (Figure 18.4II-B).[123] The functionalization of PAMAM dendrimer with triethoxysilane reduced the polymer charge density, further enabling the stable covalent-based LbL encapsulated islets to maintain high cell viability, lack foreign body responses, and enable stable normoglycemia after implantation in diabetic mice. Moreover, the LbL technique has been also employed to build hierarchically ordered 3D cellular architectures to resemble the complex and organized structure and function of native tissues. Akashi's group reported the dip-assisted LbL coating of mouse L929 fibroblast cell monolayers with FN/G nanolayers to provide a suitable cell-adhesive surface to mimic the native ECM (Figure 18.4II-C).[124] The authors reported the need for at least 6 nm thick FN/G films to act as a stable adhesive surface for adhesion of the second cell layer. Therefore, a four-layered cellular architecture has been successfully developed and envisioned to be applied for different biomedical applications.

18.4 Conclusions and Future Perspectives

Although starting with the modification and functionalization of smooth flat substrates with 2D multilayered ultrathin films more than thirty years ago, the prominent LbL assembly technology has quickly expanded to coat substrates exhibiting more complex geometries across all dimensional scales. This chapter disclosed the multitude of templates that can be used to assemble soft LbL structures for biomedical applications. Numerous examples were given on the LbL nanocoating of templates of different sizes, shapes, surface chemistry, topology, and spanning from 0D to 3D with an unprecedented array of ingredients to develop a plethora of LbL devices to fulfill a wide array of biomedical applications, including controlled drug delivery, biosensing, bioreactors, and tissue engineering and regenerative medicine. Those include inanimate 0D nanoparticles and hollow nanocapsules, 1D solid nanofibers and nanotubes, 2D flat and patterned thin films and free-standing membranes, as well as 3D architectures, including micro- and macro-particles and hollow capsules, micro- and macro-tubes, multicompartmentalized systems, porous constructs, and even dynamic and animate living cell platforms. In fact, the simplicity, cost-effectiveness, and high versatility endowed by the LbL technology are elucidated not only by the wide array of inexpensive templates and materials assembled by resorting to a multitude of intermolecular interactions, but also by the variety of methodologies that altogether enable the fabrication of a plethora of multifunctional LbL devices with fine-tuned compositions, structures, and properties at the nanometer-scale level. Hence, it comes with no surprise that LbL technology has attracted

tremendous interest in the scientific research community working across different fields. Although there are still major bottlenecks to address prior to translating the LbL technology to the clinics, noteworthily the scalability of the process, the amount and need for highly biocompatible and biodegradable materials, the use of clean rooms and strict sterilization protocols, and the huge technological developments denoted by the LbL methodology over the past decades assign it a bright future. Furthermore, the combination of its unique features with other prominent nano- and micro-technologies, such as 3D printing will enable the rational molecular design of more complex biomaterial architectures exhibiting adaptive, bioactive, and multi-stimuli responsive behavior, as well as a self-healing ability, bioinstructive behavior, and multi-scale organization, which will put the LbL technology one-step closer to reaching the clinics.

Acknowledgements

This work was supported by the Programa Operacional Regional do Centro – Centro 2020, in the component FEDER, and by national funds (OE) through FCT/MCTES, in the scope of the project ''SUPRASORT'' (PTDC/QUI-OUT/30658/2017, CENTRO-01-0145-FEDER-030658), and by the Programa Operacional Competitividade e Internacionalização (POCI), in the component FEDER, and by national funds (OE) through FCT/MCTES, in the scope of the projects ''MIMETIc'' (PTDC/BTM-MAT/31210/2017) and ''CIRCUS'' (PTDC/BTM-MAT/31064/2017). J. Borges, I.M. Bjørge and S. Nadine gratefully acknowledge FCT for the individual contract (CEECIND/03202/2017) and PhD grants (SFRH/BD/129224/2017; SFRH/BD/130194/2017), respectively. This work was also supported by the Marine Biotechnology ERA-NET project ''BLUETEETH'' (ERA-MBT/0002/2015) funded by FCT under EU FP7 (Grant Agreement number: 604814). This work was developed within the scope of the project CICECO-Aveiro Institute of Materials, UIDB/50011/2020 & UIDP/50011/2020, financed by national funds through FCT/MCTES.

References

1. R. K. Iler, *J. Colloid Interface Sci.*, 1966, **21**, 569.
2. G. Decher and J. D. Hong, *Makromol. Chem., Macromol. Symp.*, 1991, **46**, 321.
3. G. Decher, *Science*, 1997, **277**, 1232.
4. G. Decher and J. D. Hong, *Ber. Bunsenges. Phys. Chem.*, 1991, **95**, 1430.
5. J. Borges and J. F. Mano, *Chem. Rev.*, 2014, **114**, 8883.
6. R. R. Costa and J. F. Mano, *Chem. Soc. Rev.*, 2014, **43**, 3453.
7. P. T. Hammond, *Mater. Today*, 2012, **15**, 196.
8. Z. Tang, Y. Wang, P. Podsiadlo and N. A. Kotov, *Adv. Mater.*, 2006, **18**, 3203.
9. J. J. Richardson, M. Björnmalm and F. Caruso, *Science*, 2015, **348**, aaa2491.

10. Y. Wang, A. S. Angelatos and F. Caruso, *Chem. Mater.*, 2008, **20**, 848.
11. G. Schneider and G. Decher, *Nano Lett.*, 2004, **4**, 1833.
12. G. Schneider, G. Decher, N. Nerambourg, R. Praho, M. H. V. Werts and M. Blanchard-Desce, *Nano Lett.*, 2006, **6**, 530.
13. A. Elbakry, A. Zaky, R. Liebl, R. Rachel, A. Goepferich and M. Breunig, *Nano Lett.*, 2009, **9**, 2059.
14. J. Huang, Q. Shu, L. Wang, H. Wu, A. Y. Wang and H. Mao, *Biomaterials*, 2015, **39**, 105.
15. J.-F. Berret, N. Schonbeck, F. Gazeau, D. El Kharrat, O. Sandre, A. Vacher and M. Airiau, *J. Am. Chem. Soc.*, 2006, **128**, 1755.
16. X. Hong, J. Li, M. Wang, J. Xu, W. Guo, J. Li, Y. Bai and T. Li, *Chem. Mater.*, 2004, **16**, 4022.
17. A. Sexton, P. G. Whitney, S.-F. Chong, A. N. Zelikin, A. P. R. Johnston, R. De Rose, A. G. Brooks, F. Caruso and S. J. Kent, *ACS Nano*, 2009, **3**, 3391.
18. Y. Wang and F. Caruso, *Chem. Mater.*, 2005, **17**, 953.
19. Z. Poon, J. B. Lee, S. W. Morton and P. T. Hammond, *Nano Lett.*, 2011, **11**, 2096.
20. A. Ivanova, K. Ivanova, A. Tied, T. Heinze and T. Tzanov, *Adv. Funct. Mater.*, 2020, **30**, 2001284.
21. G. B. Sukhorukov, E. Donath, H. Lichtenfeld, E. Knippel, M. Knippel, A. Budde and H. Möhwald, *Colloids Surf., A*, 1998, **137**, 253.
22. C. Cortez, E. Tomaskovic-Crook, A. P. R. Johnston, A. M. Scott, E. C. Nice, J. K. Heath and F. Caruso, *ACS Nano*, 2007, **1**, 93.
23. M. K. Park, S. Deng and R. C. Advincula, *Langmuir*, 2005, **21**, 5272.
24. M. Motiei, V. Sedlařík, L. A. Lucia, H. Fei and L. Münster, *Carbohydr. Polym.*, 2020, **231**, 115709.
25. D. Trau, W. Yang, M. Seydack, F. Caruso, N.-T. Yu and R. Renneberg, *Anal. Chem.*, 2002, **74**, 5480.
26. Z. Liang, A. S. Susha, A. Yu and F. Caruso, *Adv. Mater.*, 2003, **15**, 1849.
27. S. Hou, J. Wang and C. R. Martin, *J. Am. Chem. Soc.*, 2005, **127**, 8586.
28. Q. He, W. Song, H. Möhwald and J. Li, *Langmuir*, 2008, **24**, 5508.
29. S. Hou, J. Wang and C. R. Martin, *Nano Lett.*, 2005, **5**, 231.
30. T. Komatsu, H. Terada and N. Kobayashi, *Chem. – Eur. J.*, 2011, **17**, 1849.
31. X. Qu and T. Komatsu, *ACS Nano*, 2010, **4**, 563.
32. P. Jiao, Y. Guo, A. Niu and X. Kang, *RSC Adv.*, 2015, **5**, 37130.
33. T. Komatsu, X. Qu, H. Ihara, M. Fujihara, H. Azuma and H. Ikeda, *J. Am. Chem. Soc.*, 2011, **133**, 3246.
34. T. Komatsu, *Nanoscale*, 2012, **4**, 1910.
35. S. Zhang, S. Demoustier-Champagne and A. M. Jonas, *Biomacromolecules*, 2015, **16**, 2382.
36. G. Lu, S. Ai and J. Li, *Langmuir*, 2005, **21**, 1679.
37. D. Zhang, S. A. Dougherty and J. Liang, *J. Nanopart. Res.*, 2011, **13**, 1563.
38. Q. He, Y. Tian, Y. Cui, H. Möhwald and J. Li, *J. Mater. Chem.*, 2008, **18**, 748.
39. Y. Yang, Q. He, L. Duan, Y. Cui and J. Li, *Biomaterials*, 2007, **28**, 3083.

40. W. Wang, Z. Wu, X. Lin, T. Si and Q. He, *J. Am. Chem. Soc.*, 2019, **141**, 6601.
41. H. Liang, F. Sheng, B. Zhou, Y. Pei, B. Li and J. Li, *Int. J. Biol. Macromol.*, 2017, **102**, 218.
42. K. Müller, J. F. Quinn, A. P. R. Johnston, M. Becker, A. Greiner and F. Caruso, *Chem. Mater.*, 2006, **18**, 2397.
43. B. Ding, J. Gong, J. Kim and S. Shiratori, *Nanotechnology*, 2005, **16**, 785.
44. B. Park, W. Lee, E. Lee, S. H. Min and B.-S. Kim, *ACS Appl. Mater. Interfaces*, 2015, **7**, 3329.
45. K.-f. Ren, M. Hu, H. Zhang, B. C. Li, W. X. Lei, J. Y. Chen, H. Chang, L. M. Wang and J. Ji, *Prog. Polym. Sci.*, 2019, **92**, 1.
46. M. Criado-Gonzalez, M. Fernandez-Gutierrez, J. S. Roman, C. Mijangos and R. Hernández, *Carbohydr. Polym.*, 2019, **206**, 428.
47. G. Decher, J. D. Hong and J. Schmitt, *Thin Solid Films*, 1992, **210–211**, 831.
48. L. Wu, C. Wu, G. Liu, N. Liao, F. Zhao, X. Yang, H. Qu, B. Peng, L. Chen and G. Yang, *Appl. Surf. Sci.*, 2016, **389**, 395.
49. S. Park, D. Choi, H. Jeong, J. Heo and J. Hong, *Mol. Pharmaceutics*, 2017, **14**, 3322.
50. S. Park, J. Park, J. Heo, S. E. Lee, J. W. Shin, M. Chang and J. Hong, *J. Ind. Eng. Chem.*, 2018, **68**, 229.
51. K. Jayakumar, M. B. Camarada, V. Dharuman, R. Rajesh, R. Venkatesan, H. Ju, M. Maniraj, A. Rai, S. R. Barman and Y. Wen, *ACS Appl. Mater. Interfaces*, 2018, **10**, 21541.
52. J. Borges, M. P. Sousa, G. Cinar, S. G. Caridade, M. O. Guler and J. F. Mano, *Adv. Funct. Mater.*, 2017, **27**, 1605122.
53. S. Zahouani, L. Hurman, M. De Giorgi, C. Vigier-Carrière, F. Boulmedais, B. Senger, B. Frisch, P. Schaaf, P. Lavalle and L. Jierry, *Nanoscale*, 2017, **9**, 18379.
54. J. M. Silva, J. R. García, R. L. Reis, A. J. García and J. F. Mano, *Acta Biomater.*, 2017, **51**, 279.
55. Y. Cho and J. Hong, *Colloids Surf., A*, 2019, **562**, 296.
56. V. Fitzpatrick, L. Fourel, O. Destaing, F. Gilde, C. Albigès-Rizo, C. Picart and T. Boudou, *Sci. Rep.*, 2017, **7**, 41479.
57. A. I. Neto, N. L. Vasconcelos, S. M. Oliveira, D. Ruiz-Molina and J. F. Mano, *Adv. Funct. Mater.*, 2016, **26**, 2745.
58. D. Chen, J. Chen, M. Wu, H. Tian, X. Chen and J. Sun, *Langmuir*, 2013, **29**, 8328.
59. X. Hu, E. McIntosh, M. G. Simon, C. Staii and S. W. Thomas III, *Adv. Mater.*, 2016, **28**, 715.
60. P. Ott, K. Trenkenschuh, J. Gensel, A. Fery and A. Laschewsky, *Langmuir*, 2010, **26**, 18182.
61. S. S. Ono and G. Decher, *Nano Lett.*, 2006, **6**, 592.
62. J. Sun, C. Su, X. Zhang, W. Yin, J. Xu and S. Yang, *Langmuir*, 2015, **31**, 5147.

63. R. Polak, T. Crouzier, R. M. Lim, K. Ribbeck, M. M. Beppu, R. N. M. Pitombo, R. E. Cohen and M. F. Rubner, *Biomacromolecules*, 2014, **15**, 3093.
64. J. L. Lutkenhaus, K. D. Hrabak, K. McEnnis and P. T. Hammond, *J. Am. Chem. Soc.*, 2005, **127**, 17228.
65. J. R. Rodrigues, N. M. Alves and J. F. Mano, *RSC Adv.*, 2016, **6**, 75988.
66. M. P. Sousa, A. I. Neto, T. R. Correia, S. P. Miguel, M. Matsusaki, I. J. Correia and J. F. Mano, *Biomater. Sci.*, 2018, **6**, 1962.
67. J. Borges, S. G. Caridade, J. M. Silva and J. F. Mano, *Macromol. Rapid Commun.*, 2015, **36**, 405.
68. J. M. Silva, S. G. Caridade, R. L. Reis and J. F. Mano, *Soft Matter*, 2016, **12**, 1200.
69. N. I. Martins, M. P. Sousa, C. A. Custódio, V. C. Pinto, P. J. Sousa, G. Minas, F. Cleymand and J. F. Mano, *Acta Biomater.*, 2017, **57**, 313.
70. M. P. Sousa, S. G. Caridade and J. F. Mano, *Adv. Healthcare Mater.*, 2017, **6**, 1601462.
71. C. Ribeiro, J. Borges, A. M. S. Costa, V. M. Gaspar, V. D. Z. Bermudez and J. F. Mano, *Molecules*, 2018, **23**, 625.
72. R. R. Costa, A. Girotti, M. Santos, F. J. Arias, J. F. Mano and J. C. Rodríguez-Cabello, *Acta Biomater.*, 2014, **10**, 2653.
73. A. Yashchenok, B. Parakhonskiy, S. Donatan, D. Kohler, A. Skirtach and H. Möhwald, *J. Mater. Chem. B*, 2013, **1**, 1223.
74. O. Shchepelina, I. Drachuk, M. K. Gupta, J. Lin and V. V. Tsukruk, *Adv. Mater.*, 2011, **23**, 4655.
75. Z. She, M. N. Antipina, J. Li and G. B. Sukhorukov, *Biomacromolecules*, 2010, **11**, 1241.
76. F. Huang, W. C. Liao, Y. S. Sohn, R. Nechushtai, C.-H. Lu and I. Willner, *J. Am. Chem. Soc.*, 2016, **138**, 8936.
77. L. Pastorino, E. Dellacasa, P. Petrini and O. Monticelli, *Mater. Sci. Eng., C*, 2017, **76**, 1129.
78. S. Nadine, S. G. Patrício, C. R. Correia and J. F. Mano, *Biofabrication*, 2019, **12**, 015005.
79. N. Doshi, A. S. Zahr, S. Bhaskar, J. Lahann and S. Mitragotri, *Proc. Natl. Acad. Sci. U. S. A.*, 2009, **106**, 21495.
80. R. J. R. W. Peters, M. Marguet, S. Marais, M. W. Fraaije, J. C. M. van Hest and S. Lecommandoux, *Angew. Chem., Int. Ed.*, 2014, **53**, 146.
81. J. P. Douliez, A. Perro and L. Béven, *ChemBioChem*, 2019, **20**, 2546.
82. B. Wong, C. Boyer, C. Steinbeck, D. Peters, J. Schmidt, R. van Zanten, B. Chmelka and J. A. Zasadzinski, *Adv. Mater.*, 2011, **23**, 2320.
83. X. Liu, P. Formanek, B. Voit and D. Appelhans, *Angew. Chem., Int. Ed.*, 2017, **56**, 16233.
84. B. Städler, R. Chandrawati, A. D. Price, S.-F. Chong, K. Breheney, A. Postma, L. A. Connal, A. N. Zelikin and F. Caruso, *Angew. Chem., Int. Ed.*, 2009, **48**, 4359.

85. L. Hosta-Rigau, B. Städler, Y. Yan, E. C. Nice, J. K. Heath, F. Albericio and F. Caruso, *Adv. Funct. Mater.*, 2010, **20**, 59.
86. C. Y. Yoo, J. S. Seong and S. N. Park, *Colloids Surf., B*, 2016, **144**, 99.
87. L. Hosta-Rigau, S. F. Chung, A. Postma, R. Chandrawati, B. Städler and F. Caruso, *Adv. Mater.*, 2011, **23**, 4082.
88. R. Chandrawati, B. Städler, A. Postma, L. A. Connal, S.-F. Chong, A. N. Zelikin and F. Caruso, *Biomaterials*, 2009, **30**, 5988.
89. P. A. Beales and T. K. Vanderlick, *J. Phys. Chem. B*, 2009, **113**, 13678.
90. M. Yu, W. Song, F. Tian, Z. Dai, Q. Zhu, E. Ahmad, S. Guo, C. Zhu, H. Zhong, Y. Yuan, T. Zhang, X. Yi, X. Shi, Y. Gan and H. Gao, *Proc. Natl. Acad. Sci. U. S. A.*, 2019, **116**, 5362.
91. B. G. De Geest, S. De Koker, K. Immesoete, J. Demeester, S. C. De Smedt and W. E. Hennink, *Adv. Mater.*, 2008, **20**, 3687.
92. R. R. Costa, E. Castro, F. J. Arias, J. C. Rodríguez-Cabello and J. F. Mano, *Biomacromolecules*, 2013, **14**, 2403.
93. H. Bäumler and R. Georgieva, *Biomacromolecules*, 2010, **11**, 1480.
94. A. Postma, Y. Yan, Y. Wang, A. N. Zelikin, E. Tjipto and F. Caruso, *Chem. Mater.*, 2009, **21**, 3042.
95. J. M. Silva, A. R. C. Duarte, C. A. Custódio, P. Sher, A. I. Neto, A. C. M. Pinho, J. Fonseca, R. L. Reis and J. F. Mano, *Adv. Healthcare Mater.*, 2014, **3**, 433.
96. J. M. Silva, C. A. Custódio, R. L. Reis and J. F. Mano, *ACS Biomater. Sci. Eng.*, 2016, **2**, 2304.
97. A. F. Colino, F. Wolf, R. Moreira, S. Rütten, T. Schmitz-Rode, J. C. Rodríguez-Cabello, S. Jockenhoevel and P. Mela, *Eur. Polym. J.*, 2019, **121**, 109334.
98. R. W. N. Nugroho, K. Odelius, A. Höglund and A.-C. Albertsson, *Chem. Mater.*, 2016, **28**, 3298.
99. O. S. Manoukian, A. Aravamudhan, P. Lee, M. R. Arul, X. Yu, S. Rudraiah and S. G. Kumbar, *ACS Biomater. Sci. Eng.*, 2018, **4**, 2181.
100. P. Sher, C. R. Correia, R. R. Costa and J. F. Mano, *RSC Adv.*, 2015, **5**, 2511.
101. P. Sher, S. M. Oliveira, J. Borges and J. F. Mano, *Biofabrication*, 2015, **7**, 011001.
102. C. R. Correia, I. M. Bjørge, J. Zeng, M. Matsusaki and J. F. Mano, *Adv. Healthcare Mater.*, 2019, **8**, 1901221.
103. W. Hu, Z. Wang, Y. Zha, X. Gu, W. You, Y. Xiao, X. Wang, S. Zhang and J. Wang, *Adv. Healthcare Mater.*, 2020, 2000035.
104. Y. Qian, L. Li, Y. Song, L. Dong, P. Chen, X. Li, K. Cai, O. Germershaus, L. Yang and Y. Fan, *Biomaterials*, 2018, **164**, 22.
105. K. Ramalingam, R. Castro, P. Pires, X. Shi, J. Rodrigues, S. Xiao and H. Tomás, *RSC Adv.*, 2016, **6**, 97116.
106. P. Gentile, A. M. Ferreira, J. T. Callaghan, C. A. Miller, J. Atkinson, C. Freeman and P. V. Hatton, *Adv. Healthcare Mater.*, 2017, **6**, 1601182.
107. S. M. Oliveira, R. L. Reis and J. F. Mano, *ACS Biomater. Sci. Eng.*, 2015, **1**, 2.

108. Y. Yan, H. Chen, H. Zhang, C. Guo, K. Yang, K. Chen, R. Cheng, N. Qian, N. Sandler, Y. S. Zhang, H. Shen, J. Qi, W. Cui and L. Deng, *Biomaterials*, 2019, **190–191**, 97.
109. Q. Tang, Z. Hu, H. Jin, G. Zheng, X. F. Yu, G. Wu, H. Liu, Z. Zhu, H. Xu, C. Zhang and L. Shen, *Theranostics*, 2019, **9**, 1125.
110. B. J. Zhang, L. He, Z. W. Han, X. G. Li, W. Zhi, W. Zheng, Y. D. Mu and J. Weng, *J. Mater. Chem. B*, 2017, **5**, 8238.
111. Z. Guo, N. Jiang, J. Moore, C. P. McCoy, M. Ziminska, C. Rafferty, G. Sarri, A. R. Hamilton, Y. Li, L. Zhang, S. Zhu and D. Sun, *ACS Appl. Mater. Interfaces*, 2019, **11**, 27269.
112. T. Zhou, L. Yan, C. Xie, P. Li, L. Jiang, J. Fang, C. Zhao, F. Ren, K. Wang, Y. Wang, H. Zhang, T. Guo and X. Lu, *Small*, 2019, **15**, 1805440.
113. M. B. Oliveira, J. Hatami and J. F. Mano, *Chem. – Asian J.*, 2016, **11**, 1753.
114. R. F. Fakhrullin and Y. M. Lvov, *ACS Nano*, 2012, **6**, 4557.
115. A. C. Anselmo, K. J. McHugh, J. Webster, R. Langer and A. Jaklenec, *Adv. Mater.*, 2016, **28**, 9486.
116. H. C. Moon, S. Han, J. Borges, T. Pesqueira, H. Choi, S. Y. Han, H. Cho, J. H. Park, J. F. Mano and I. S. Choi, *Soft Matter*, 2020, **16**, 6063.
117. G. Liu, L. Li, D. Huo, Y. Li, Y. Wu, L. Zeng, P. Cheng, M. Xing, W. Zeng and C. Zhu, *Biomaterials*, 2017, **127**, 117.
118. G. Wang, T. Zhao, X. Song, W. Zhong, L. Yu, W. Hua, M. M. Q. Xing and X. Qiu, *Polym. Chem.*, 2015, **6**, 283.
119. J. T. Wilson, W. Cui, V. Kozlovskaya, E. Kharlampieva, D. Pan, Z. Qu, V. R. Krishnamurthy, J. Mets, V. Kumar, J. Wen, Y. Song, V. V. Tsukruk and E. L. Chaikof, *J. Am. Chem. Soc.*, 2011, **133**, 7054.
120. V. Kozlovskaya, O. Zavgorodnya, Y. Chen, K. Ellis, H. M. Tse, W. Cui, J. A. Thompson and E. Kharlampieva, *Adv. Funct. Mater.*, 2012, **22**, 3389.
121. R. F. Schwabe and C. Jobin, *Nat. Rev. Cancer*, 2013, **13**, 800.
122. M. T. Speth, U. Repnik and G. Griffiths, *Biomaterials*, 2016, **111**, 1.
123. K. M. Gattás-Asfura, N. J. Abuid, I. Labrada and C. L. Stabler, *ACS Biomater. Sci. Eng.*, 2020, **6**, 2641.
124. M. Matsusaki, K. Kadowaki, Y. Nakahara and M. Akashi, *Angew. Chem., Int. Ed.*, 2007, **46**, 4689.